Lecture 12
Multiplet splitting

Multiplet splitting

Atomic → various L and S terms

Both valence and core levels

Rare earths

Transition metals

Paramagnetic free molecules

Consider 3s level emission from Mn2+ free ion ground state of Mn^{2+} is $3s^2\ 3d^5\ {}^6S$ (S = 5/2, L = 0)

3s emission gives two final states,

$3s^1\ 3d^5$ ^5S(S=2, L=0) and ^7S (S=3, L=0)

spins coupled antiparallel — spins coupled parallel

Exchange interaction acts when electrons are coupled parallel ^7S has lower energy than ^5S due to 3s-3d exchange.

The energy separation between the states will be proportional to Exchange integral $K_{3s,3d}$

$\Delta E_b(3s) = E^f(3s\ 3d^5\ ^7S) = \Delta E^f(3s3d^5)$

A Hatree Fock calculation for the equation gives ΔE^f as 13 eV. The experimental shifts are one half the theoretical value possibly due to correlation.

Example: Mn^{2+} photoemission, 3s and 3p

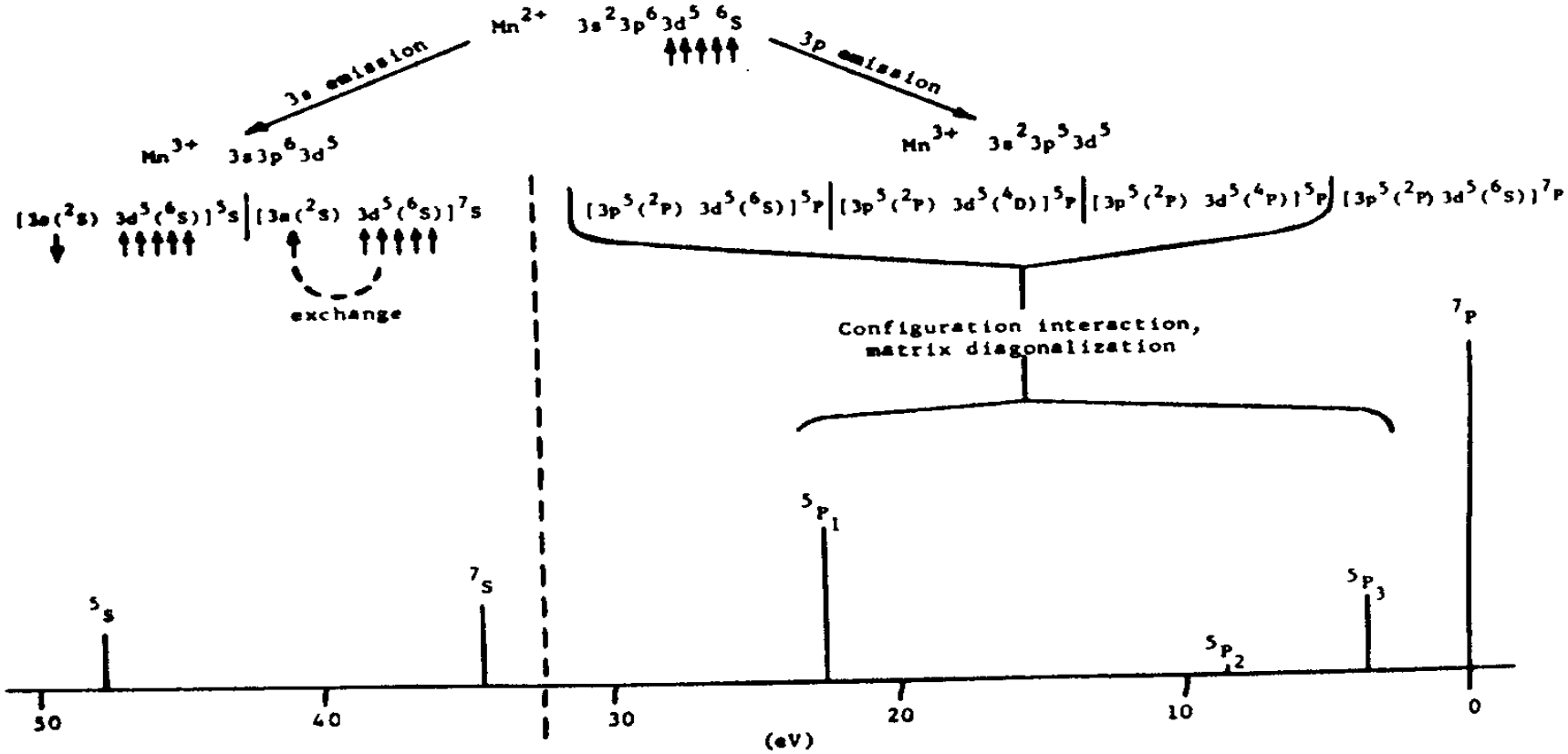

Fig. 30. The various final state L, S multiplets arising from $3s$ and $3p$ photoemission from a Mn^{2+} ion. Within the S and P manifolds, separations and relative intensities have been computed using simple atomic multiplet theory as discussed in the text. The separation and relative intensity of the ^7S and ^7P peaks were fixed at the values observed for $3s(1)$ and $3p(1)$ in the MnF_2 spectrum of Fig. 31 to facilitate comparison with experiment. (From Fadley, ref. 262.)

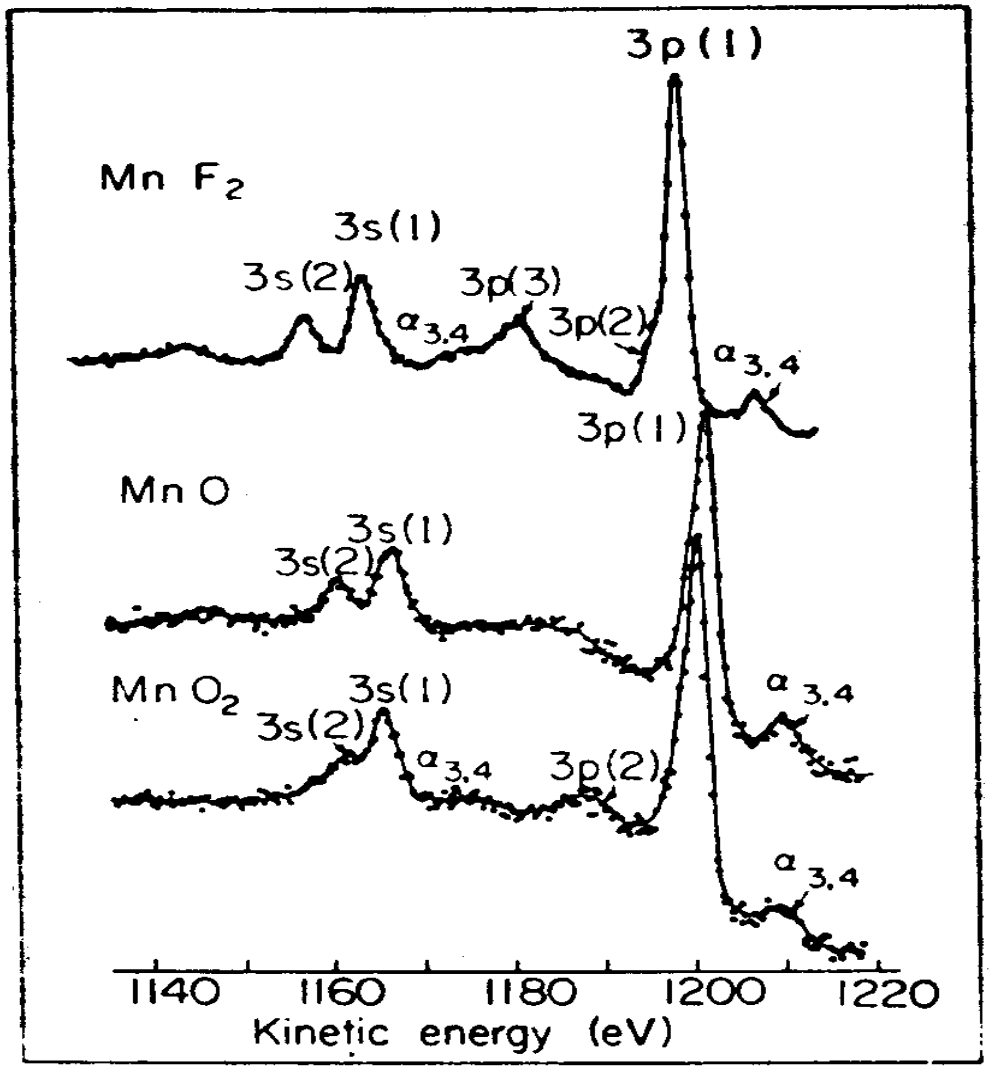

Fig. 31. XPS spectra from three solid compounds containing Mn, in the kinetic energy region corresponding to emission of Mn3*s* and 3*p* electrons. The initial-state ions present are $Mn^{+2}3d^5$ (MnF_2, MnO) and $Mn^{+4}3d^3$ (MnO_2). Peaks due to multiplet splittings are labelled 3*s*(1), 3*s*(2), etc. $K\alpha_{3,4}$ x-ray satellite structures are also indicated. (From Fadley and Shirley, ref. 86.)

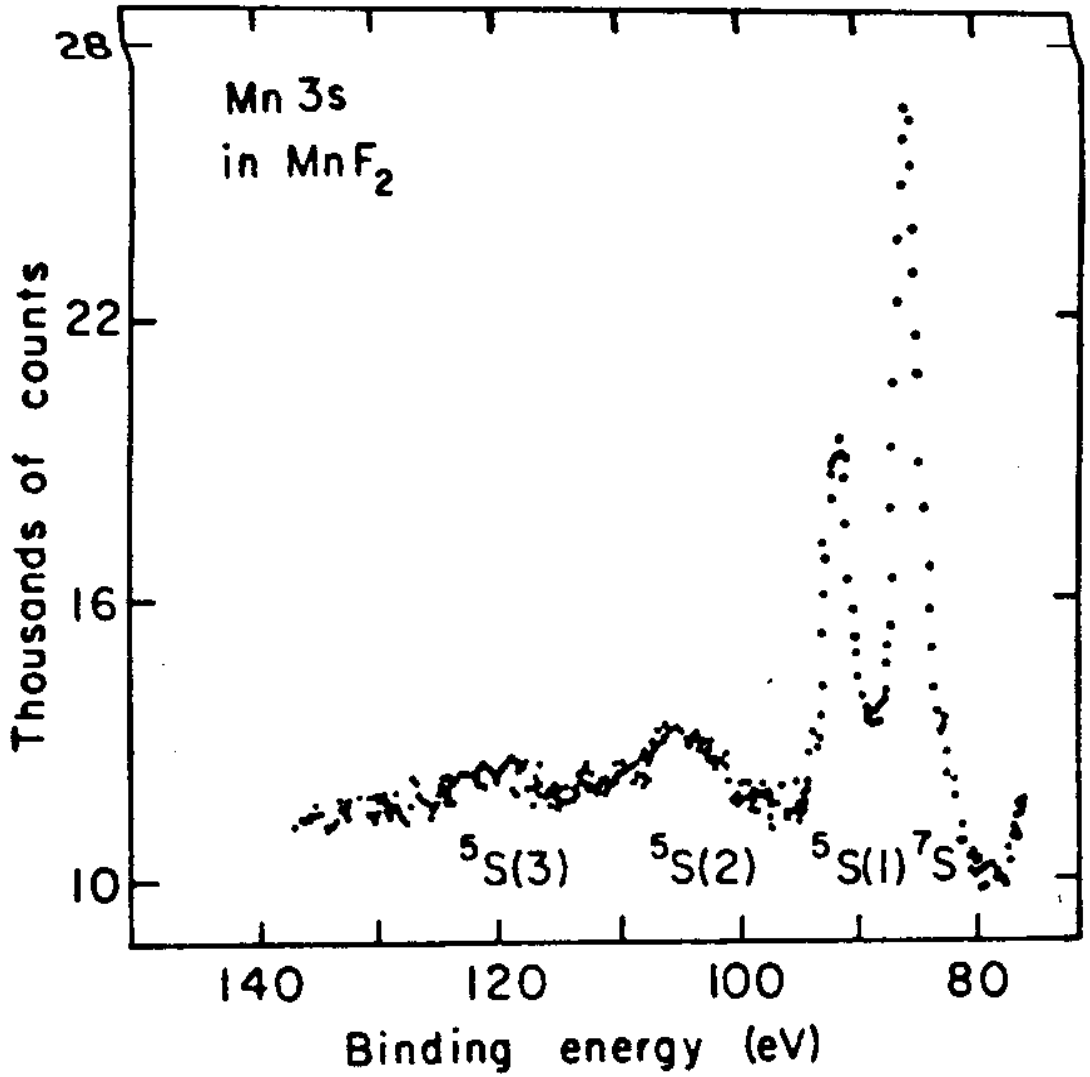

Fig. 33. Higher resolution Mn3*s* spectrum from MnF_2 obtained with monochromatized AlKα radiation (cf. Fig. 31). The peaks $^5S(2)$ and $^5S(3)$ arise from final-state configuration interaction (correlation effects) according to Eq. (151). (From Kowalczyk *et al.*, ref. 253.)

Although it is enough to have one set of orbitals, in predicting the absolute energies and intensities ,configuration interaction calculations are needed.

The ^7S state was found to consist almost entirely of the one electron configuration, $\phi_1(^7S) = 3s^1(^2S)\ 3p^6(^1S)\ 3d^5(^6S)$

Which is the one electron configuration

The ^5S state is composed of other configurations too.

$\phi_1(^5S) = 3s^1(^2S)\ 3p^6(^1S)\ 3d^5(^6S)$

$\phi_2(^5S) = 3s^2(^1S)\ 3p^4(^3P)\ 3d^6(^3P)$

$\phi_3(^5S) = 3s^2(^1S)\ 3p^2(^3P)\ 3d^6(^3P)$

$\phi_4(^5S) = 3s^2(^1S)\ 3p^4(^1D)\ 3d^6(^5D)$

Thus there will be at least four peaks for the ^5S state one of these states lie close in energy w.r.t ^7S state. That is the reason why the one electron estimate of 13 eV is not seen experimentally. Only three distinct ^5S states are observed.

Similar splittings are observed in paramagnetic molecules such as NO and O_2. The N_{ls} and O_{ls} show splitting of 1.5 and 1.1 eV. The splitting is proportional to the exchange integral between unfilled valence molecular orbital and the ls ortibal of N or O.

For a non s emission the final states are more complex.

The core hole $(nl)^{q-1}$ can have a spin ½ and have non zero orbital angular momentum. This can couple with a valence level of $(n'l')^{p}$ (with spin S" and orbital angular momentum L"). The number of final states increases. There can be complexities due to spin orbit splitting and crystal field splitting.

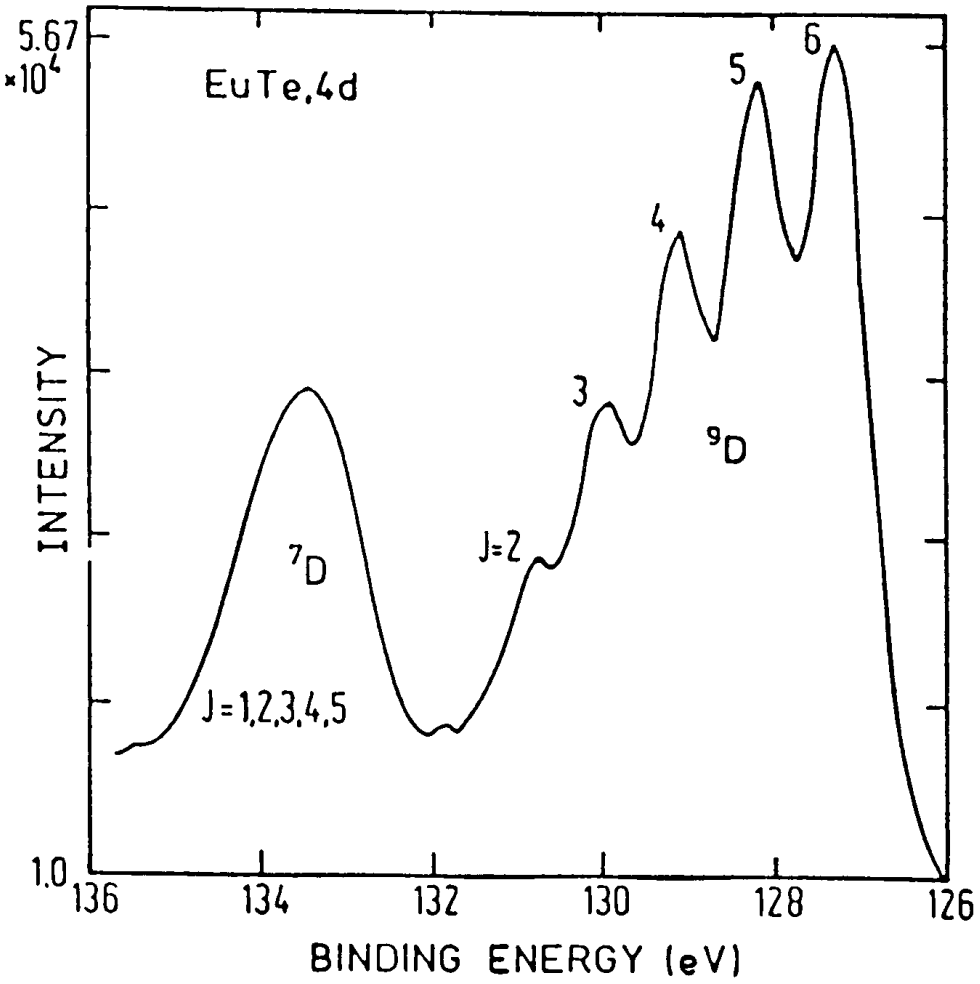

4d core line of Eu in EuTe (Eu^{2+}). The $^2d_{3/2}$ and $^2d_{5/2}$ final hole state couple to the $^8S_{7/2}$ state of the 4f electrons yielding a $^7D_{1...5}$ multiplet and a $^9D_{2...6}$ multiplet.

Consider 3p emission from Mn^{2+},

$(nl)^{q-1} = 3p^5\ (n'l')^p = 3d^5$

Initial state is ^6S ($S = 5/2$, $L=0$)

The selection rule $\Delta l = l^f - l = \pm 1$

$\Delta S = S^f - S = \pm 1/2$

$\Delta L = L^f - L = 0, \pm 1, \pm 2 \ldots \pm l$ or

$L_f = L+l, L+l-l, \ldots, |L-l|$

The allowed final state is ^5P, but it can be reached by three ways. i.e., by the following coupling schemes.

$3p^5(S = ½, l=1)$ with $3d^5$ ^6S ($S"=5/2$, $L" = 0$)

$3p^5(S = ½, l=1)$ with $3d^5$ ^4D ($S" = 3/2$, $L"= 2$)

$3p^5(S = ½, l=1)$ with $3d^5$ ^4P ($S' = 3/2$, $L" = 1$)

There is another final state, viz ^7P. Thus there will be four distinct states. One ^7P and three ^5P.

Such effects are seen in deeper core levels also but the effect will be less pronounced since the strength of the interaction decreases. These effects are also seen in valence levels, especially systems containing unfilled 4f levels.

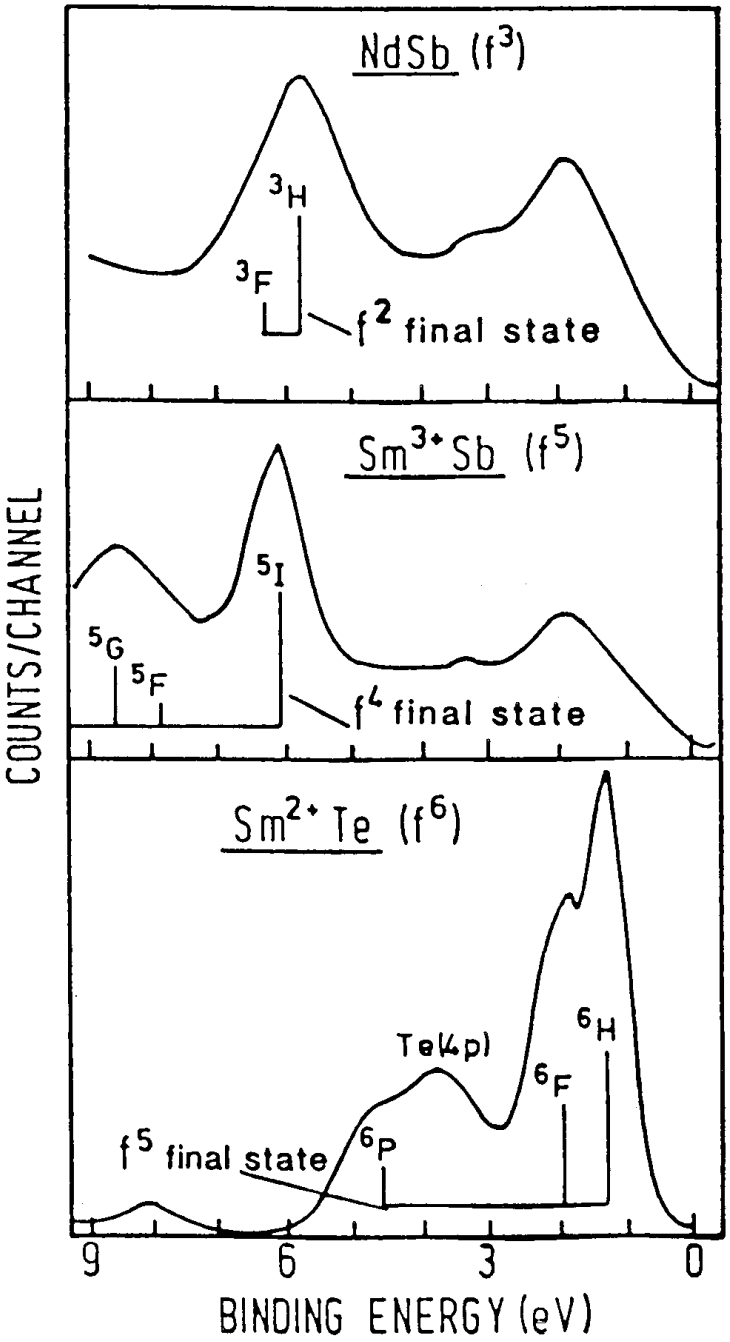

XPS valence band spectra of (from top to bottom): $Nd^{3+}Sb$ (initial state $4f^3$), the $4f^2$ final state is well separated from the valence band; $Sm^{3+}Sb$ (initial state $4f^5$), the $4f^4$ final state is well separated from the valence band near the Fermi energy; $Sm^{2+}Te$ (initial state $4f^6$), here the $4f^5$ final state is near the Fermi energy due to the additional 4f electron.

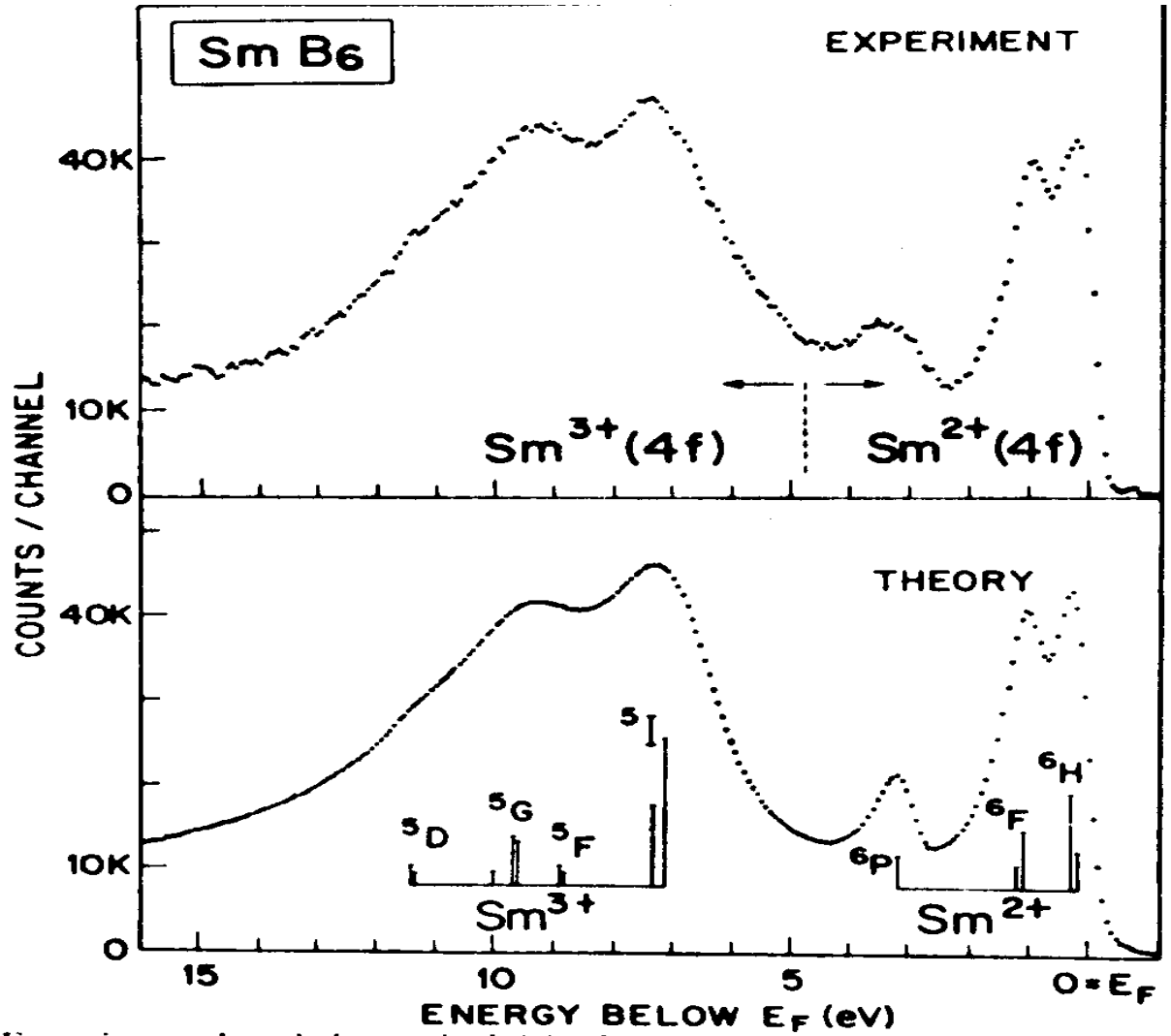

Fig. 35. Experimental and theoretical $4f$ valence spectra from SmB_6, a "mixed-valence" metallic compound believed to contain both $Sm^{+2}\ 4f^6$ and $Sm^{+3}\ 4f^5$. The intensities of the various final-state multiplets for $Sm^{+2} \rightarrow Sm^{+3}$ and $Sm^{+3} \rightarrow Sm^{+4}$ were computed using fractional parentage coefficients and are indicated as vertical bars. These calculations were broadened by an empirically-derived function of the form of Eq. (158) to generate the final theoretical curve. Monochromatized AlKα was used for excitation. (From Chazalviel *et al.*, ref. 266.)

Multiplet: Molecules

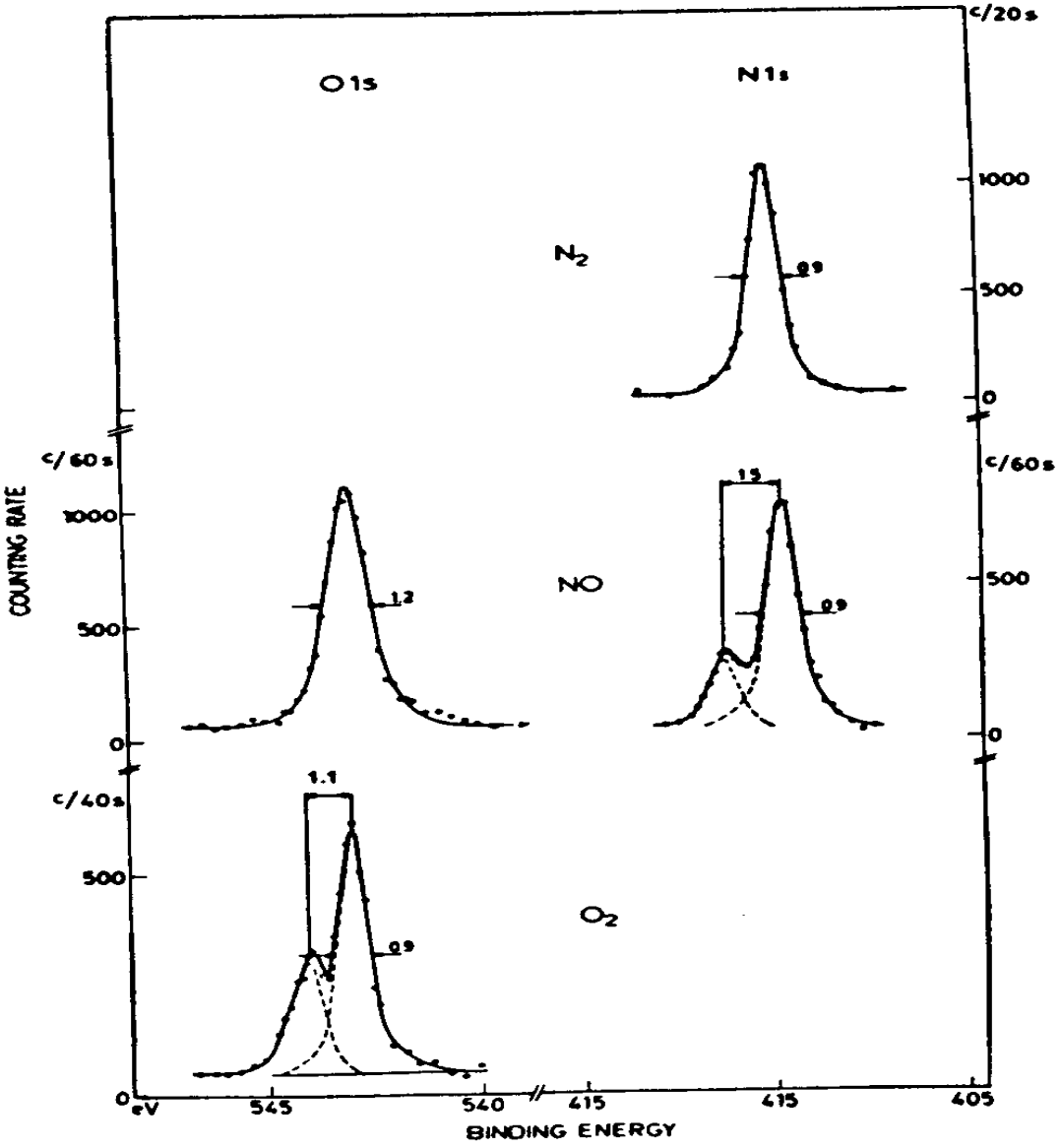

Fig. 34. XPS spectra from the 1*s* core electrons of the gaseous molecules N_2, NO, and O_2. The 1*s* peaks from the paramagnetic molecules NO and O_2 are split due to final-state multiplets. Diamagnetic N_2 shows no splitting. (From Siegbahn *et al.*, ref. 4.)

Multi-electron excitations

No transition is one-electron. Relaxation does occur and all transitions are indeed multi electron. But the multi electron effects are judged against purely one electron description where in no relaxation occurs.

Shake-up, Shake-off and related correlation effects

Both two and three electron processes occur. Two electron events are approximately 10 times greater in intensity.

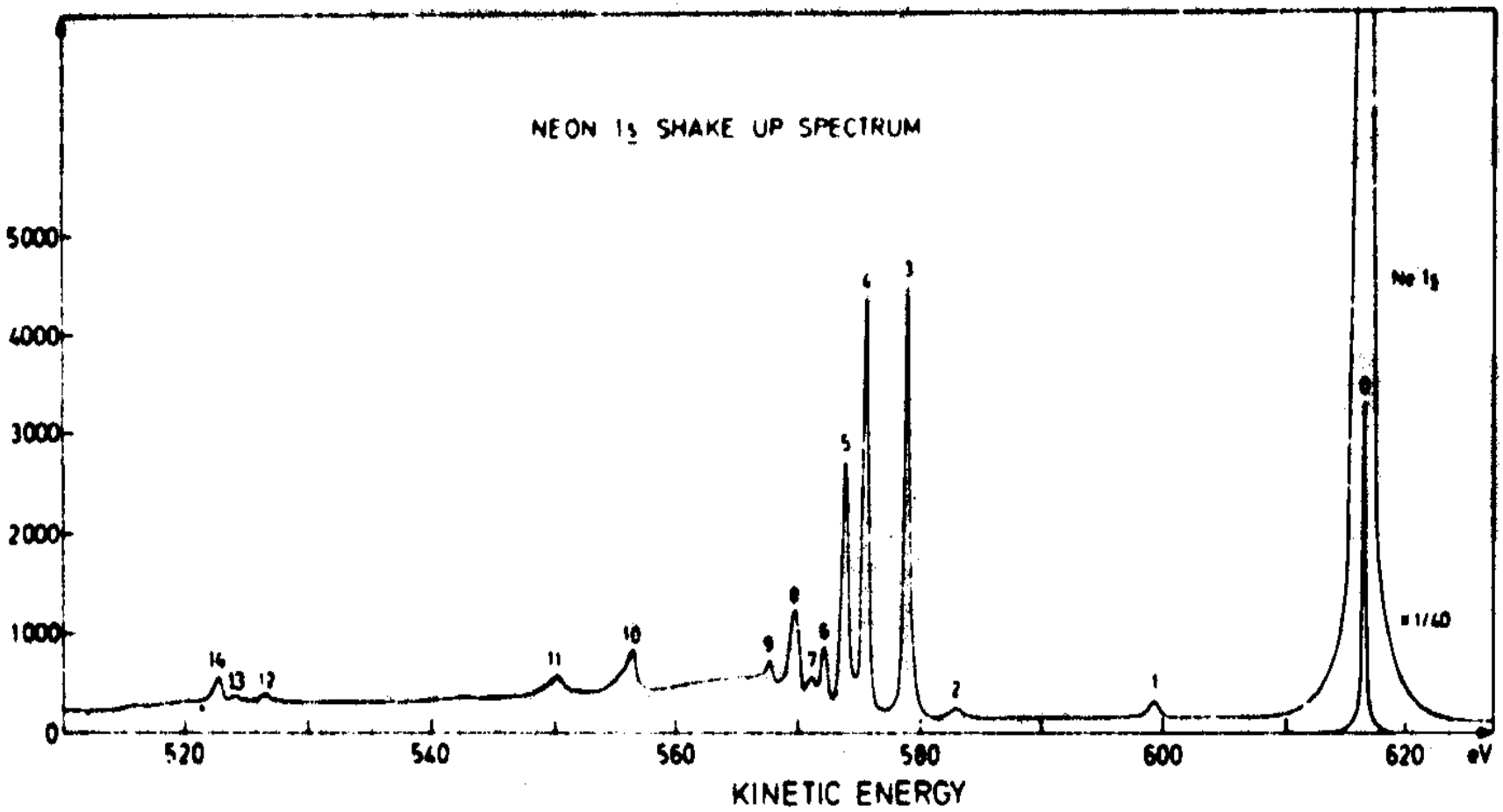

Fig. 36. High-resolution shake-up spectrum associated with excitation from Nels in gaseous neon. Table II lists the origins of the various satellite peaks labelled 1–14. The Nels FWHM was reduced to 0·4 eV in these measurements by using a monochromatized AlKα source. (From Gelius, ref. 270.)

Shake-up

$$(nl)^q\,(n'l')^p \longrightarrow (nl)^{q-1}(n'l')^{p-1}(n'',l'')^1 + e^- \text{ photoelectron}$$

Shake-off

$$(nl)^q(n'l')^p \longrightarrow (nl)^{q-1}\,(n'l')^{p-1}\,(E_{kin},l'')' + e^- \text{ photoelectron}$$

The primary electron loses energy.

Such shake-ups are seen in molecules also

Multi electron transition in metals

Due to the availability of states with continuous energy below Fermi level, the discrete Satellites in molecular become an asymmetric tail in solids. Such line shape can be calculated.

We also get plasmon excitation ‘intrinsic’ during PE emission event, ‘extrinsic’ – during photoelectron escape.

Core peak satellites in transition metal and rare earth compounds

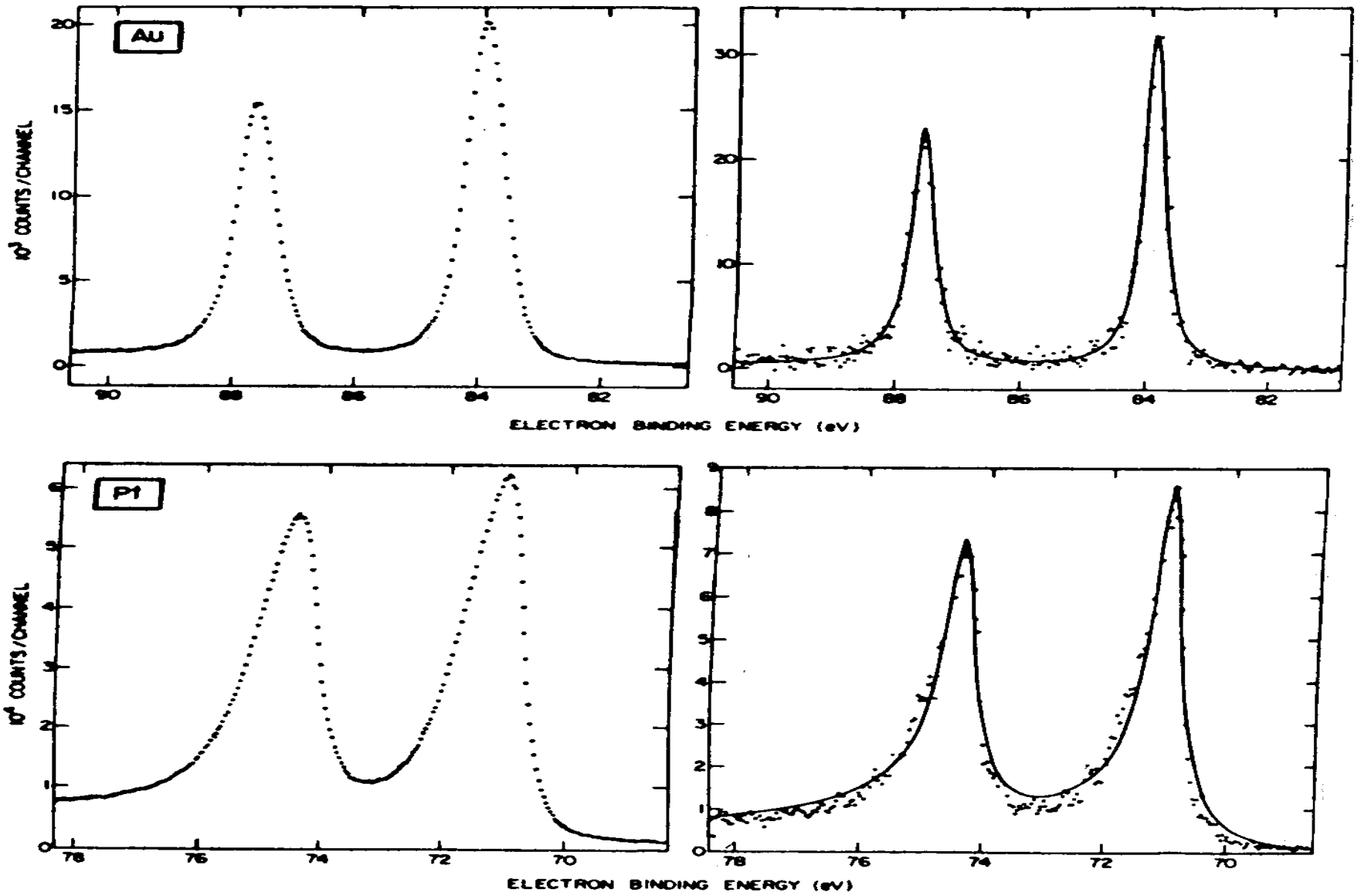

Fig. 37. 4*f* core spectra from polycrystalline Au and Pt (points) in comparison to a best fit of the asymmetric line shape predicted by Eq. (158) (curves). In the right panels, the data have been corrected by deconvolution of the instrumental line shape, but no correction for inelastic scattering effects has been made. The instrumental line shape was derived from the form of the cut-off near E_F (cf. Fig. 13). (From Hüfner and Wertheim, ref. 84.)

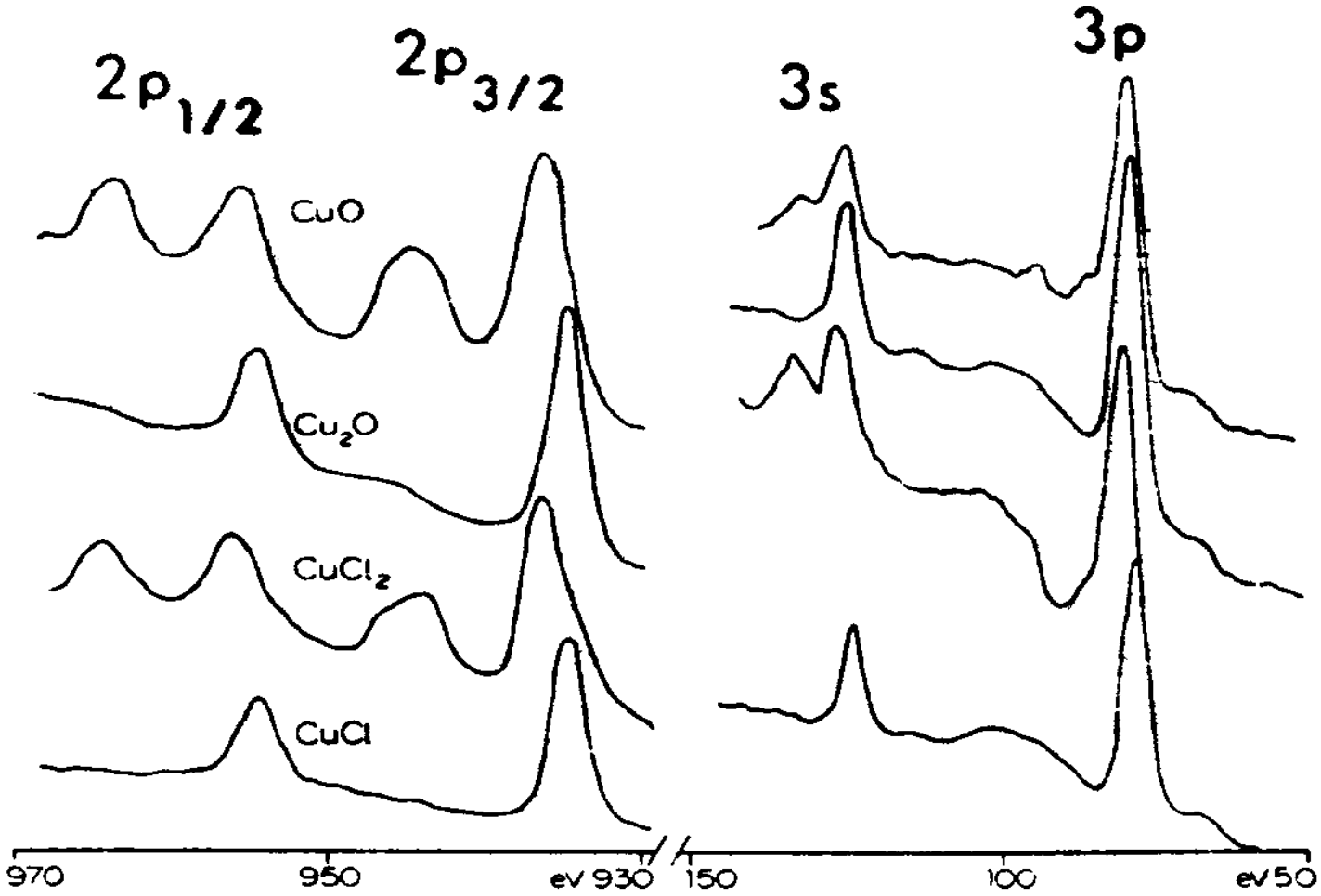

Fig. 38. $2p_{\frac{1}{2}}$, $\frac{1}{2}$ and $3s$, $3p$ core-level spectra from the copper compounds CuO, Cu_2O, $CuCl_2$, and CuCl. The low-energy satellites are very strong in Cu^{-2} $3d^9$ compounds (CuO, $CuCl_2$), and very weak in Cu^{-1} $3d^{10}$ compounds (Cu_2O, CuCl). (From Frost *et al.*, ref. 281.)

Core peak satellites

In Cu2p core level, strong low KE satellites are observed in Cu^{2+} ($3d^9$) compounds are very weak in Cu^{1+}($3d^{10}$) compounds. The satellites are very strong, comparable to the one electron peaks.

This is supposed to involve ligand to metal charge transfer. This results in $3d^{n+1}$ or $4f^{n+1}$ configuration. This is a possible relaxation mechanism. Possibly the reason why 3d or 4f filled states do not show such satellites. The core-hole wave function is written as a combination of two configurations. One configuration involved charge transfer and other no charge transfer in an octahedral environment the CT configuration is assumed to have an electron transfer from eg(bonding) to eg(anti bonding) eg^b is basically ligand and eg^a is metal d^n.

ϕ_1 = (core hole) $(eg^b)^n$ $(eg^a)^m$
ϕ_2 = (core hole) $(eg^b)^{n-1}$ $(eg^a)^{m+1}$

Mixing these configurations give two final states with differing degrees of charge transfer.

$\Psi_1^f = C_{11}\,\phi_1 + C_{12}\,\phi_2$ at E_1^f
$\Psi_2^f = C_{21}\,\phi_1 + C_{22}\,\phi_2$ at E_2^f

Ψ_1^f is taken as the main line:
crystal field effects, multiplet effects
and spin orbit interactions give further fine structure.

Adsorption of CO.
Satellites in finger printing

Other multi electron effects

For elements with Z = 50-60, the 4p spectrum is broad and is a result of many electron resonance. After 4p emission, the configurations are …$4p^5 4d^{10} 5s^2$… The exact outer configuration depends on Z. 4d BE is approximately ½ of 4p. Thus one 4d electron can be moved to 4p and another can be placed in band unoccupied or continuum orbital we get a set of configurations like …$4p^6 4d^8 5s^2$ …$(n"l")^1$ or …$4p^6 4d^8 5s^2$ …$(E_{kin}"l")^1$ and these are nearly degenerate with one electron final state. Strong mixing of these states give broad resonances.

There can be complexities due to Coster-Kronig de excitations.
4d $\rightarrow$4p, 4d $\rightarrow$ continuum.

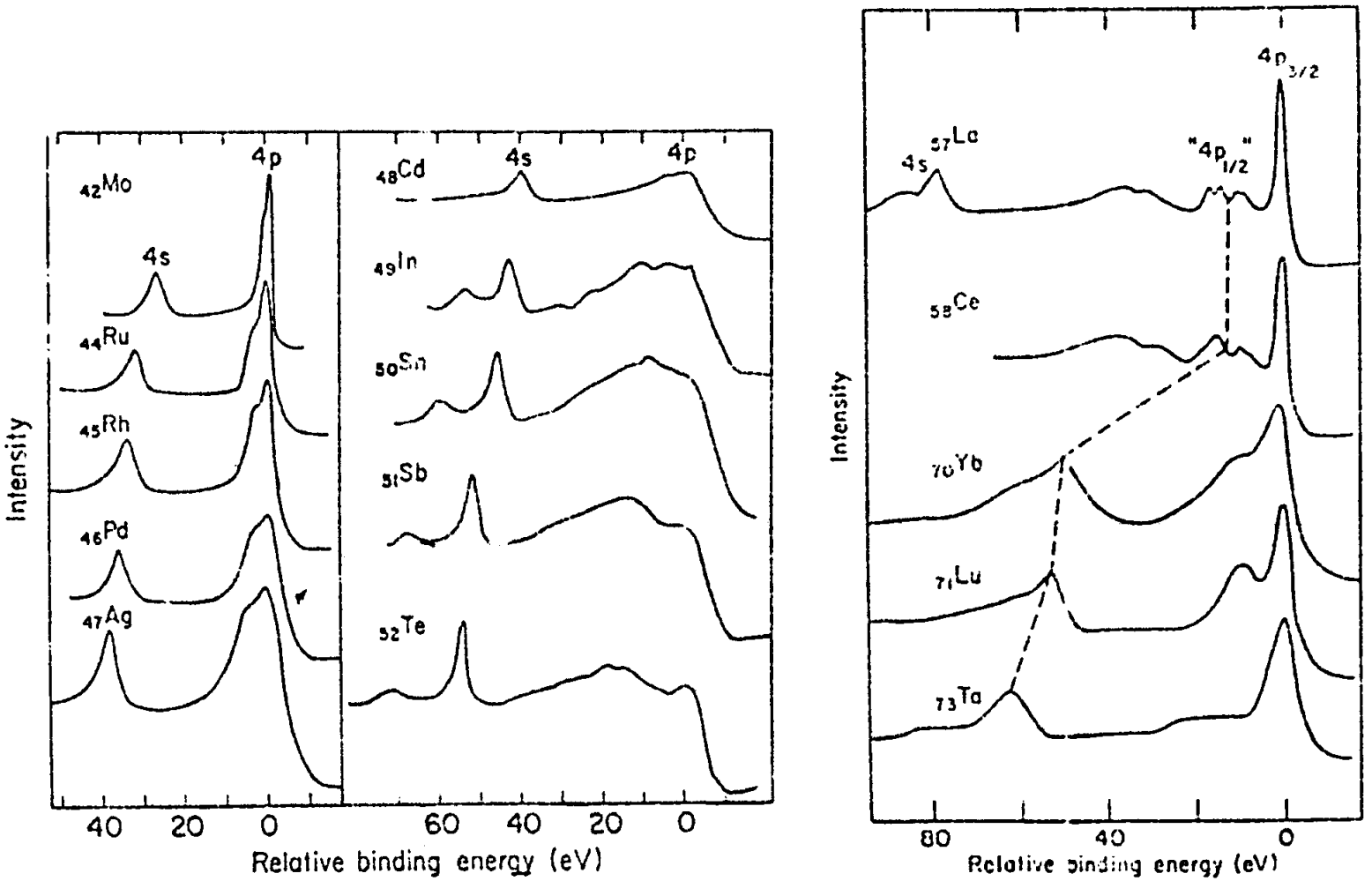

Fig. 39. 4*s*, 4*p* core-level spectra for a series of metals from Mo ($Z=42$) to Ta ($Z=73$). Note the broad 4*p* resonance that exists from $Z\approx 49$ to $Z\gtrsim 60$. (From Shirley *et al.*, ref. 215.)

Vibrational Effects

Methane spectrum
Spectra of potassium halides

Angle resolved measurements

a) Surface sensitivity enhancement of grafing exit angles

$$d = \Lambda_e \sin \theta$$

Silicon surface
Aluminium surface

b) Surface sensitivity enhancement at grazing x-ray incidence angles. Refraction at the surface is significant at $\phi_x \leq 1^0$, when $\phi_x > 1^0$, the x-ray penetration depth is about 10^3-10^5Å. For $\phi_x \leq 1^0$, the penetration depth is comparable with Λ_e. Refraction makes $\phi_x' << \phi_x$.

Vibrational excitation

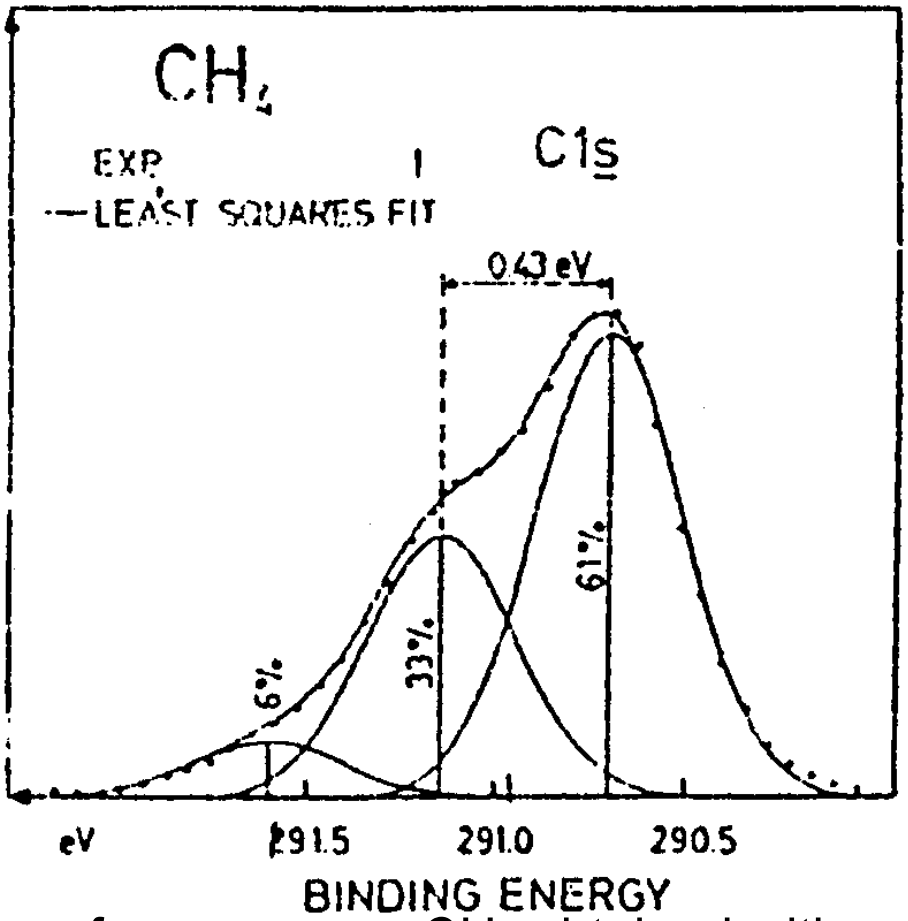

A Cls spectrum from gaseous CH_4 obtained with very high instrumental resolution (FWHM ≈ 0.3eV). The lowest-binding-energy primary peak shown here is found to exhibit three components due to vibrational excitations in the final state.

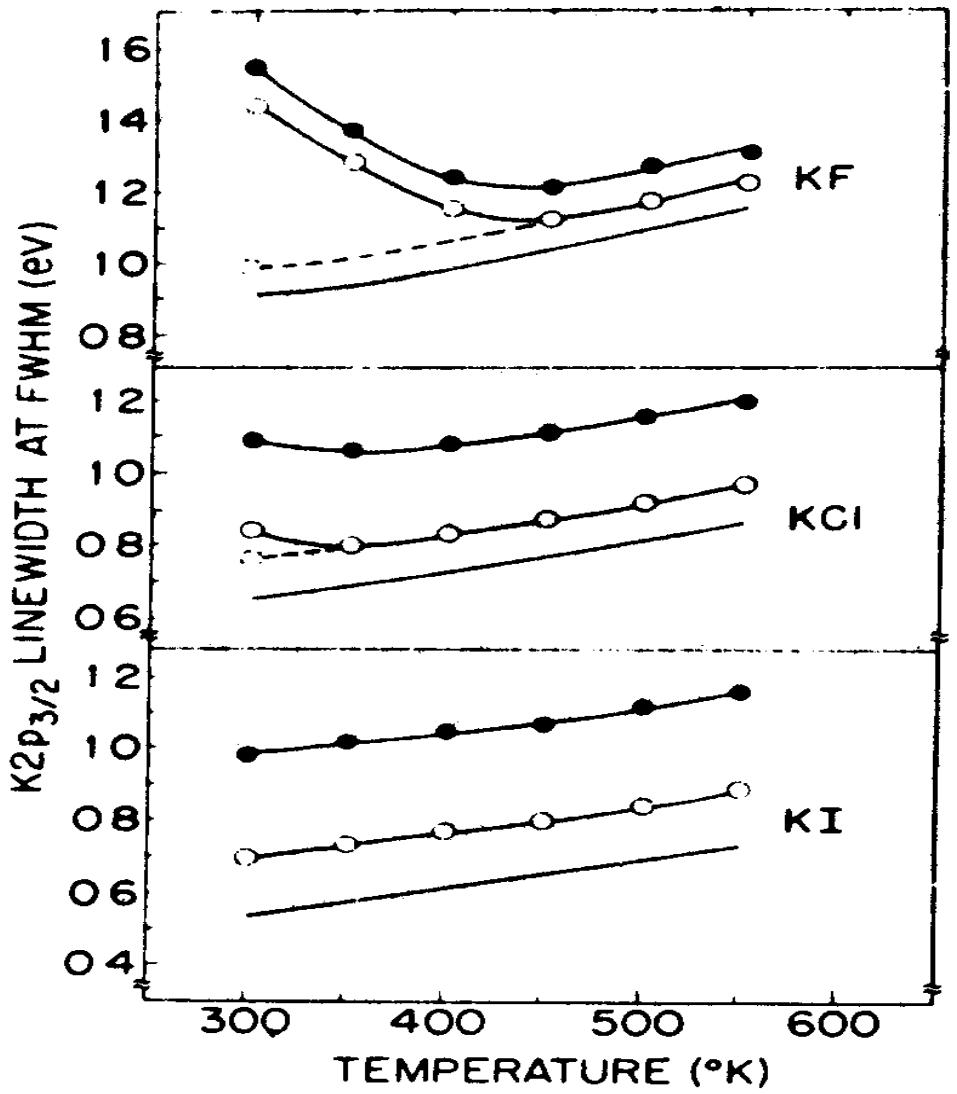

Fig. 41. Variation of the K2$p_{\frac{3}{2}}$ FWHM with temperature in solid KF, KCl, and KI. the curves —●—●— are the unaltered experimental data. The curves —○—○— have been corrected for lifetime and instrumental width contributions. The dotted curves represent further corrections for specimen charging that occurred in KF and KI at low temperatures. The solid curves are theoretical calculations based upon final-state vibrational broadening. (From Citrin *et al.*, ref. 85.)

Surface sensitivity

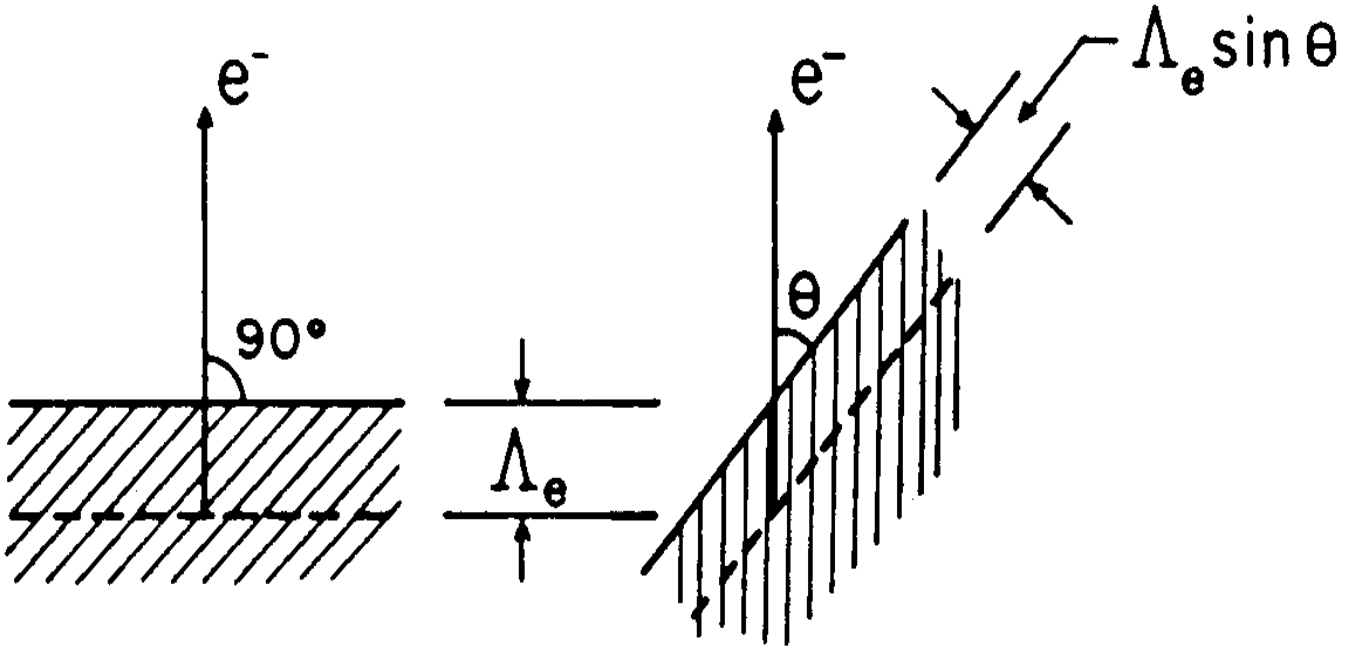

$$5\,\text{Å} \lesssim \Lambda_e \lesssim 80\,\text{Å}$$

Fig. 43. Illustration of the basic mechanism producing surface sensitivity enhancement for low electron exit angles θ. The average depth for no-loss emission as measured perpendicular to the surface is given by $\Lambda_e \sin\theta$.

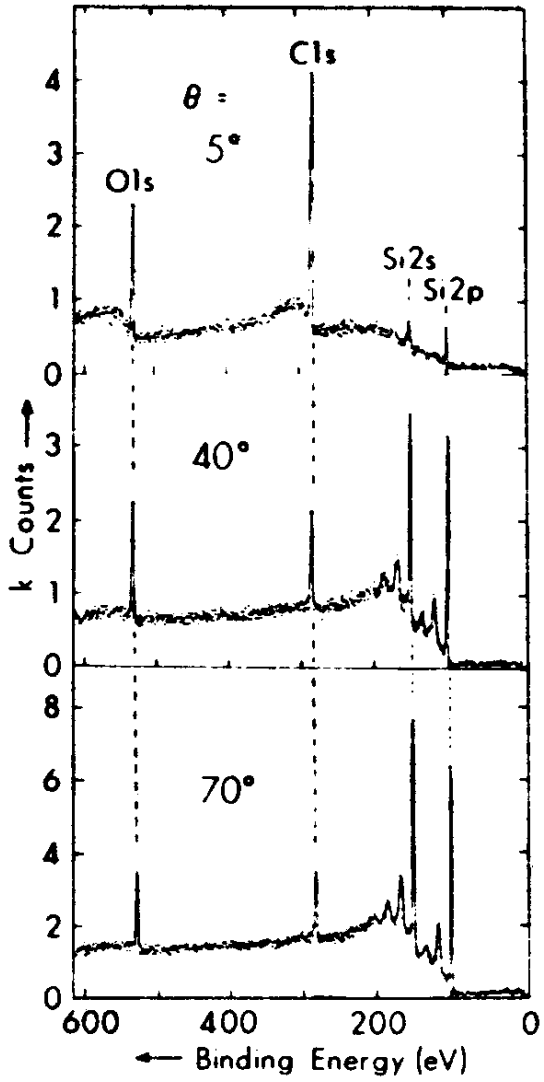

Fig. 44. Broad-scan core spectra at low and high exit angles for a Si specimen with a thin oxide overlayer (~4 Å) and an outermost carbon contaminant overlayer approximately 1–2 monolayers in thickness. The C1*s* and O1*s* signals are markedly enhanced in relative intensity at low θ due to the general effect presented in Fig. 43. (From Fadley, ref. 17.)

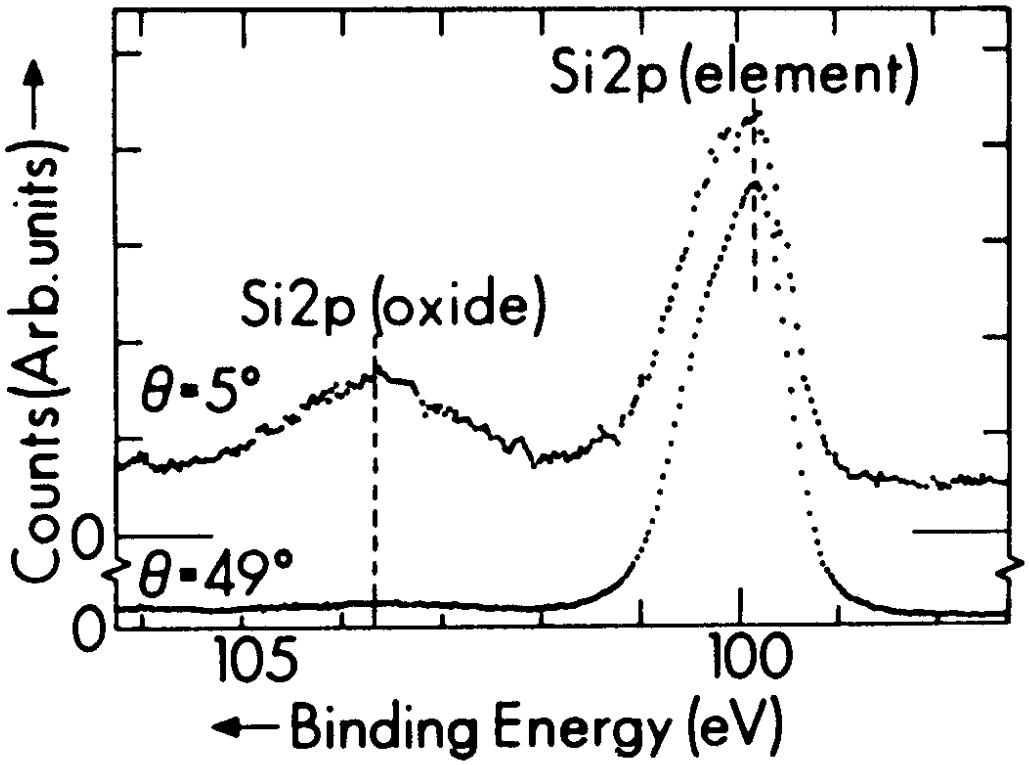

Fig. 45. Si2*p* core spectra at $\theta = 5°$ and 49° for the specimen of Fig. 44. The chemically-shifted Si2*p* (oxide) peak is enhanced in relative intensity by approximately a factor of 20 between 49° and 5°. (From Fadley, ref. 17.)

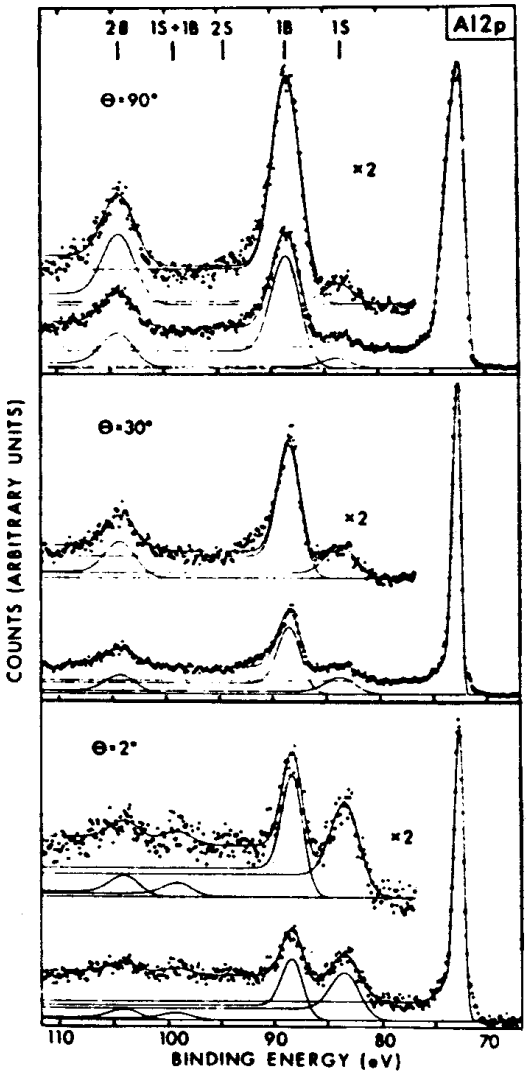

Fig. 46. A12*p* plasmon loss spectra from a clean surface of polycrystalline aluminium at $\theta = 90°$, 30°, and 2°. The positions of various combinations of surface and bulk losses are denoted 1S, 1B, etc. Note the marked enhancement of the relative intensity of the surface plasmon loss (1S) for grazing exit angles. (From Baird *et al.*, ref. 295.)

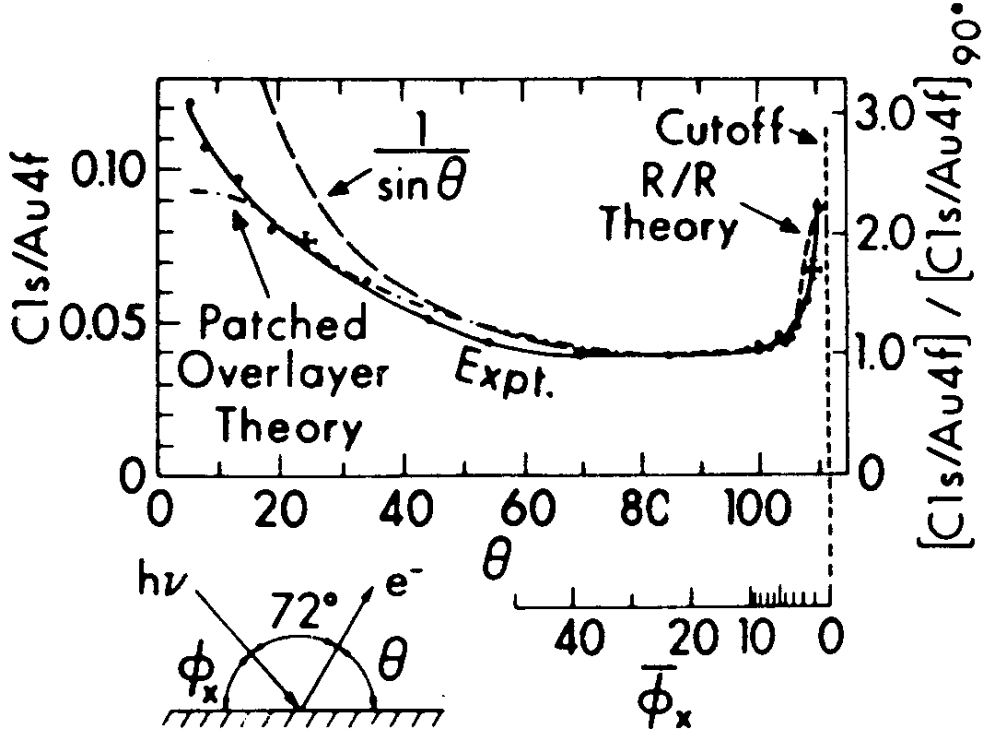

Fig. 48. Angular dependence of the C1*s*/Au4*f* intensity ratio for a gold specimen with a thin carbon-containing overlayer. Enhancement of the near-surface carbon signal is found for both grazing electron exit (low θ) and grazing x-ray incidence (low ϕ_x). The low-ϕ_x enhancement is well predicted by classical calculations allowing for x-ray refraction and reflection (R/R) at the surface, as shown by the dashed curve. (From Mehta and Fadley, ref. 179.)

Single Crystal Effects

Electron channeling	10^4-10^6 eV
Kikuchi bands	$\geq$ 300 eV

Valence band spectra also show similar effects.